Available online at www.sciencedirect.com
SCIENCE DIRECT®
International Journal of Solids and Structures 43 (2006) 4906–4916
INTERNATIONAL JOURNAL OF SOLIDS and STRUCTURES
www.elsevier.com/locate/ijsolstr

A viscoplastic strain gradient analysis of materials with voids or inclusions

Ulrik Borg [a], Christian F. Niordson [a,*], Norman A. Fleck [b], Viggo Tvergaard [a]

[a] *Department of Mechanical Engineering, Solid Mechanics, Technical University of Denmark, Nils Koppels Alle, Building 404, Kgs, Lyngby, DK-2800, Denmark*
[b] *Department of Engineering, Cambridge University, Cambridge, UK*

Received 7 April 2005; received in revised form 19 May 2005
Available online 27 July 2005

Abstract

A finite strain viscoplastic nonlocal plasticity model is formulated and implemented numerically within a finite element framework. The model is a viscoplastic generalisation of the finite strain generalisation by Niordson and Redanz (2004) [Journal of the Mechanics and Physics of Solids 52, 2431–2454] of the strain gradient plasticity theory proposed by Fleck and Hutchinson (2001) [Journal of the Mechanics and Physics of Solids 49, 2245–2271]. The formulation is based on a viscoplastic potential that enables the formulation of the model so that it reduces to the strain gradient plasticity theory in the absence of viscous effects. The numerical implementation uses increments of the effective plastic strain rate as degrees of freedom in addition to increments of displacement. To illustrate predictions of the model, results are presented for materials containing either voids or rigid inclusions. It is shown how the model predicts increased overall yield strength, as compared to conventional predictions, when voids or inclusions are in the micron range. Furthermore, it is illustrated how the higher order boundary conditions at the interface between inclusions and matrix material are important to the overall yield strength as well as the material hardening.

Keywords: Strain gradient plasticity; Viscoplastic material; Voids; Size effects

1. Introduction

A number of small scale experiments for metals have shown that size-effects play an important role when strain gradients become large (Fleck et al., 1994; Ma and Clarke, 1995; Stölken and Evans, 1998; Haque

* Corresponding author. Tel.: +45 4525 4287; fax: +45 4593 1475.
E-mail address: cn@mek.dtu.dk (C.F. Niordson).

0020-7683/$ - see front matter © 2005 Elsevier Ltd. All rights reserved.
doi:10.1016/j.ijsolstr.2005.05.022

and Saif, 2003). Such effects are not accounted for in conventional plasticity theories, and several nonlocal material models have been developed to incorporate the influence of a characteristic material length.

For a gradient plasticity theory proposed by Fleck and Hutchinson (2001) a finite strain generalisation has recently been developed by Niordson and Redanz (2004) and a numerical implementation for power law hardening materials has been given by Niordson and Tvergaard (2005). This finite strain model has been used to study necking instabilities in tension as well as buckling instabilities in compression. It was found that the gradient effects delay the onset of localisation and increase the load carrying capacity in compression, in agreement with bifurcation results of Benallal and Tvergaard (1995). Very recently also the effect of the gradient plasticity theory on the occurrence of cavitation instabilities has been analysed (Niordson and Tvergaard, in press). As is known from previous studies (Fleck and Hutchinson, 1997; Huang et al., 2000; Tvergaard and Niordson, 2004), the role of void growth is much reduced when the void radius is small compared to the characteristic material length. This results in an increased peak stress for cavitation, but subsequently the stress decays, as the void grows large relative to the material length scale.

In a viscoplastic theory for isotropic materials strain gradient effects have been incorporated by Gurtin (2003) in a small strain formulation. Also Gudmundson (2004) has proposed a small deformation strain gradient plasticity theory that has an elastic–viscoplastic version, and these viscoplastic constitutive relations have been applied by Fredriksson and Gudmundson (2005) to analyse pure shear and biaxial strain of a thin film.

In the present paper a viscoplastic version of the finite strain model of Niordson and Redanz (2004) is formulated, i.e. a viscoplastic finite strain generalisation of the gradient plasticity theory proposed by Fleck and Hutchinson (2001). This formulation makes use of a viscoplastic potential and the viscous material behaviour is introduced in terms of a power law expression for a nonlocal effective plastic strain rate. Since, in the viscoplastic theory, no internal boundaries exists between elastic and plastic regions, no internal higher order boundary conditions must be specified. Such internal boundary conditions are necessary in a time-independent theory. To illustrate predictions of this viscoplastic nonlocal model, numerical results are presented for elastic–viscoplastic materials containing either voids or rigid inclusions. The results show the effect of different values of the void or inclusion radius relative to the characteristic material length incorporated in the theory. For the material with inclusions different higher order boundary conditions at the inclusion surface are investigated.

2. Material model

Let u_i denote the displacement vector and $\dot{u}_i$ the velocity field. With $\dot{e}_{ij} = \dot{u}_{i,j}$ denoting the velocity gradient, the material spin is given by

$$\dot{\omega}_{ij} = \frac{1}{2}(\dot{e}_{ij} - \dot{e}_{ji}) \tag{1}$$

The symmetric part of the velocity gradient is the strain rate, which is decomposed into an elastic and plastic part

$$\dot{\epsilon}_{ij} = \frac{1}{2}(\dot{e}_{ij} + \dot{e}_{ji}) = \dot{\epsilon}^{\mathrm{E}}_{ij} + \dot{\epsilon}^{\mathrm{P}}_{ij} \tag{2}$$

A nonlocal measure of the effective plastic strain rate is defined on the basis of the conventional effective plastic strain rate and the gradient of the conventional effective plastic strain rate through the incremental relation

$$\dot{E}^{\mathrm{P}^2} = \dot{\epsilon}^{\mathrm{P}^2} + l_*^2 \dot{\epsilon}^{\mathrm{P}}_{,i} \dot{\epsilon}^{\mathrm{P}}_{,i} \tag{3}$$

where l_* is a material length parameter (Fleck and Hutchinson, 2001; Niordson and Redanz, 2004).

The direction of the plastic strain rate is given by $m_{ij} = \frac{3}{2} S_{ij}/\sigma_e$, where $S_{ij} = \sigma_{ij} - \frac{1}{3}\delta_{ij}\sigma_{kk}$ denotes the stress deviator and $\sigma_e = \sqrt{\frac{3}{2} S_{ij} S_{ij}}$ is von Mises effective stress with σ_{ij} being the Cauchy stress tensor. The plastic strain rate components can then be written as a product of its magnitude, $\dot{\epsilon}^{\mathrm{P}} = \sqrt{\frac{2}{3}\dot{\epsilon}^{\mathrm{P}}_{ij}\dot{\epsilon}^{\mathrm{P}}_{ij}}$, and its direction

$$\dot{\epsilon}^{\mathrm{P}}_{ij} = m_{ij}\dot{\epsilon}^{\mathrm{P}} \tag{4}$$

Following (Fleck and Hutchinson, 2001), assuming that the plastic strain gradients contribute to the internal work, the principle of virtual power in total form may be formulated as

$$\int_V (\sigma_{ij}\delta\dot{\epsilon}_{ij} + (Q - \sigma_{(e)})\delta\dot{\epsilon}^{\mathrm{P}} + \tau_i \delta\dot{\epsilon}^{\mathrm{P}}_{,i})\mathrm{d}V = \int_S (T_i \delta\dot{u}_i + \tau_i n_i \delta\dot{\epsilon}^{\mathrm{P}})\mathrm{d}S \tag{5}$$

in the deformed configuration. Here, Q is a generalised effective stress which is work-conjugate to the conventional effective plastic strain rate, $\dot{\epsilon}^{\mathrm{P}}$, and τ_i is a higher order stress which is work-conjugate to the gradient of the conventional effective plastic strain rate, $\dot{\epsilon}^{\mathrm{P}}_{,i}$. The current volume and surface are denoted V and S, respectively. The surface traction is denoted by, $T_i = \sigma_{ij} n_j$, and $\tau_i n_i$ denotes the higher order surface traction.

We now define Kirchhoff stress measures as (defining J as the determinant of the metric tensor)

$$\varsigma_{ij} = J\sigma_{ij}, \quad \sigma^{\varsigma}_{(e)} = J\sigma_{(e)}, \quad q = JQ, \quad \rho_i = J\tau_i \tag{6}$$

Introducing the Jaumann rate of the Kirchhoff stress, $\overset{\triangledown}{\varsigma}_{ij}$, and the convected rate of the higher order Kirchhoff stress, $\overset{\vee}{\rho}_i$, the incremental version of the principle of virtual power, in an updated Lagrangian framework, can be expressed as (Niordson and Redanz, 2004)

$$\int_V (\overset{\triangledown}{\varsigma}_{ij}\delta\dot{\epsilon}_{ij} - \sigma_{ij}(2\dot{\epsilon}_{ik}\delta\dot{\epsilon}_{kj} - \dot{e}_{kj}\delta\dot{e}_{ki}) + (\dot{q} - \dot{\sigma}^{\varsigma}_{(e)})\delta\dot{\epsilon}^{\mathrm{P}} + \overset{\vee}{\rho}_i \delta\dot{\epsilon}^{\mathrm{P}}_{,i})\mathrm{d}V = \int_S (\dot{T}_i \delta\dot{u}_i + \dot{\rho}_i n_i \delta\dot{\epsilon}^{\mathrm{P}})\mathrm{d}S \tag{7}$$

Now, to obtain a viscoplastic version of the theory, a viscoplastic potential is defined as

$$\Phi[\dot{E}^{\mathrm{P}}, E^{\mathrm{P}}] = \int_0^{\dot{E}^{\mathrm{P}}} \sigma_{\mathrm{c}}[\dot{E}^{\mathrm{P}\prime}, E^{\mathrm{P}}]\mathrm{d}\dot{E}^{\mathrm{P}\prime} \tag{8}$$

where σ_{c} is an effective stress which is work-conjugate to the effective plastic strain rate, $\dot{E}^{\mathrm{P}}$. Taking the variation of the potential gives

$$\delta\Phi = \sigma_{\mathrm{c}}\delta\dot{E}^{\mathrm{P}} = \frac{\sigma_{\mathrm{c}}}{\dot{E}^{\mathrm{P}}}\dot{\epsilon}^{\mathrm{P}}\delta\dot{\epsilon}^{\mathrm{P}} + \frac{\sigma_{\mathrm{c}}}{\dot{E}^{\mathrm{P}}} l_*^2 \dot{\epsilon}^{\mathrm{P}}_{,i}\delta\dot{\epsilon}^{\mathrm{P}}_{,i} = q\delta\dot{\epsilon}^{\mathrm{P}} + \rho_i \delta\dot{\epsilon}^{\mathrm{P}}_{,i} \tag{9}$$

with the generalised effective stress, q, and the higher order stress, ρ_i, defined by the constitutive equations

$$q = \frac{\sigma_{\mathrm{c}}}{\dot{E}^{\mathrm{P}}}\dot{\epsilon}^{\mathrm{P}} \tag{10}$$

$$\rho_i = \frac{\sigma_{\mathrm{c}}}{\dot{E}^{\mathrm{P}}} l_*^2 \dot{\epsilon}^{\mathrm{P}}_{,i} \tag{11}$$

By substituting these expressions into the definition of the effective plastic strain (3) it is seen that the effective stress is given as the following quadratic form in q and ρ_i

$$\sigma_{\mathrm{c}}^2 = q^2 + l_*^{-2}\rho_i\rho_i \tag{12}$$

When excluding the material length scale by setting $l_* = 0$, the effective stress, σ_{c}, reduces to the von Mises stress and the effective plastic strain rate, $\dot{E}^{\mathrm{P}}$, equals the conventional effective plastic strain rate, $\dot{\epsilon}^{\mathrm{P}}$.

The viscous material behaviour is modelled by a power law for the effective plastic strain rate

$$\dot{E}^{\mathrm{P}} = \dot{\epsilon}_0 \left(\frac{\sigma_{\mathrm{c}}}{g[E^{\mathrm{P}}]} \right)^{1/m} \tag{13}$$

Here, m is the strain rate hardening exponent and $\dot{\epsilon}_0$ is a reference strain rate. Strain hardening is taken to follow a power law with exponent $1/n$ and initial yield strength $\sigma_0 = E\epsilon_0$ (where E is Young's modulus) given by

$$g[E^{\mathrm{P}}] = \sigma_0 \left(1 + \frac{E^{\mathrm{P}}}{\epsilon_0} \right)^{1/n} \tag{14}$$

where the hardening function is evaluated at E^P instead of ϵ^P as it would be in conventional J_2 flow theory. If the strain rate was prescribed such that $\dot{E}^{\mathrm{P}} = \dot{\epsilon}_0$, the hardening function, $g[E^P]$, would be equal to the effective stress, σ_{c}.

The incremental constitutive equations for the viscoplastic material can be obtained from (10) and (11) using (13) and written in the form

$$\overset{\triangledown}{\varsigma}_{ij}\Delta t = R_{ijkl}(\Delta\epsilon_{kl} - m_{kl}\Delta\epsilon^{\mathrm{P}}) = \Delta\varsigma_{ij} - \Delta\omega_{ik}\sigma_{kj} - \sigma_{ik}\Delta\omega_{jk} \tag{15}$$

$$\dot{q}\Delta t = \frac{\sigma_{\mathrm{c}}}{\dot{E}^{\mathrm{P}}} \left((m-1)\frac{\dot{\epsilon}^{\mathrm{P}}}{\dot{E}^{\mathrm{P}}}\Delta\dot{E}^{\mathrm{P}} + \Delta\dot{\epsilon}^{\mathrm{P}} \right) + \left(\frac{\dot{E}^{\mathrm{P}}}{\dot{\epsilon}_0} \right)^m \frac{\mathrm{d}g}{\mathrm{d}E^{\mathrm{P}}}\dot{\epsilon}^{\mathrm{P}}\Delta t \tag{16}$$

$$\overset{\triangledown}{\rho}_i\Delta t = l_*^2 \left(\frac{\sigma_{\mathrm{c}}}{\dot{E}^{\mathrm{P}}} \left((m-1)\frac{\dot{\epsilon}^{\mathrm{P}}_{,i}}{\dot{E}^{\mathrm{P}}}\Delta\dot{E}^{\mathrm{P}} + \Delta\dot{\epsilon}^{\mathrm{P}}_{,i} \right) + \left(\frac{\dot{E}^{\mathrm{P}}}{\dot{\epsilon}_0} \right)^m \frac{\mathrm{d}g}{\mathrm{d}E^{\mathrm{P}}}\dot{\epsilon}^{\mathrm{P}}_{,i}\Delta t \right) = \Delta\rho_i - \Delta e_{ik}\rho_k \tag{17}$$

where the change in the effective plastic strain rate is taken as $\Delta\dot{E}^{\mathrm{P}} = \frac{\dot{\epsilon}^{\mathrm{P}}}{\dot{E}^{\mathrm{P}}}\Delta\dot{\epsilon}^{\mathrm{P}} + \frac{l_*^2\dot{\epsilon}^{\mathrm{P}}_{,i}}{\dot{E}^{\mathrm{P}}}\Delta\dot{\epsilon}^{\mathrm{P}}_{,i}$ and the elastic stiffness tensor is given by

$$R_{ijkl} = \frac{E}{1+v}\left(\frac{1}{2}\left(\delta_{ik}\delta_{jl} + \delta_{il}\delta_{jk} \right) + \frac{v}{1-2v}\delta_{ij}\delta_{kl} \right) \tag{18}$$

3. Problem formulation and numerical method

A material containing uniformly distributed cylindrical voids or rigid inclusions, Fig. 1(a), is analysed using a plane strain cell model, Fig. 1(b). The dimensions of the unit cell are given by a_0 and b_0, and the size of the void or inclusion is defined by the radius R_0.

The boundary conditions used for the cell model are

$$\begin{aligned} &\dot{u}_1 = 0, \quad \dot{T}_2 = 0 \text{ at } x_1 = 0 \\ &\dot{u}_1 = \dot{U}_{\mathrm{I}}, \quad \dot{T}_2 = 0 \text{ at } x_1 = a_0 + \Delta a \\ &\dot{u}_2 = 0, \quad \dot{T}_1 = 0 \text{ at } x_2 = 0 \\ &\dot{u}_2 = \dot{U}_{\mathrm{II}}, \quad \dot{T}_1 = 0 \text{ at } x_2 = b_0 + \Delta b \end{aligned} \tag{19}$$

where $\dot{T}_i$ are surface traction rates. Using a special Rayleigh–Ritz finite element method (Tvergaard, 1976), the prescribed cell-side displacement rates, $\dot{U}_{\mathrm{I}}$ and $\dot{U}_{\mathrm{II}}$, are determined such that there is a fixed ratio of the average true stresses

$$\sigma_2 = \kappa\sigma_1 \tag{20}$$

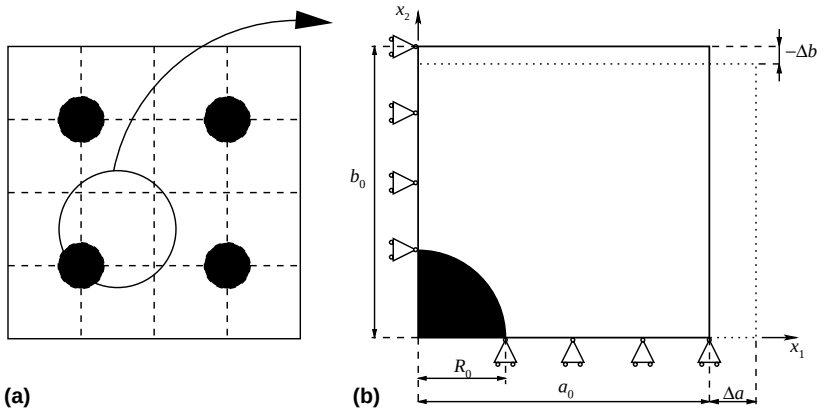

Fig. 1. The plane strain cell model for a material with rigid inclusions or voids: (a) periodically arranged inclusions/voids and (b) the unit cell used for the analyses.

Furthermore, when considering voids we have $\dot{T}_i = 0$ on the void surface, whereas in the case of inclusions we have $\dot{u}_i = 0$ on the inclusion surface.

The numerical solutions are obtained using a special kind of finite element method, where increments of the plastic strain rate appear as degrees of freedom on equal footing with displacement increments. The displacement increments, Δu_i, and the change of the effective plastic strain rate, $\Delta\dot{\epsilon}^{\mathrm{P}}$, are interpolated within each element between nodal displacement increments, ΔD^N, and nodal effective plastic strain rate changes, $\Delta\dot{\epsilon}^{\mathrm{P}}_N$, respectively

$$\Delta u_i = \sum_{N=1}^{2k} N_i^N \Delta D^N, \quad \Delta\dot{\epsilon}^{\mathrm{P}} = \sum_{N=1}^{l} M^N \Delta\dot{\epsilon}^{\mathrm{P}}_N \tag{21}$$

where N_i^N and M^N are shape functions and k and l are the number of nodes used for the interpolations. The elements used are isoparametric eight-node quadrilaterals with quadratic interpolation of both displacement increments and effective plastic strain rate increments ($k = l = 8$), as in Niordson and Tvergaard (2005) for a time independent analysis. The derivatives of the displacement increments and the effective plastic strain rate increments are taken as

$$\Delta e_{ij} = \sum_{N=1}^{2k} N^N_{i,j} \Delta D^N, \quad \Delta\epsilon_{ij} = \sum_{N=1}^{2k} E^N_{ij} \Delta D^N, \quad \Delta\dot{\epsilon}^{\mathrm{P}}_{,i} = \sum_{N=1}^{l} M^N_{,i} \Delta\dot{\epsilon}^{\mathrm{P}}_N \tag{22}$$

where $E^N_{ij} = \frac{1}{2}(N^N_{i,j} + N^N_{j,i})$.

Using these relations in the principle of virtual work, the discretized equations can be written in the following form:

$$\begin{bmatrix} \mathbf{K}_{\mathrm{e}} & \mathbf{0} \\ \mathbf{K}_{\mathrm{ep}} & \mathbf{K}_{\mathrm{p}} \end{bmatrix} \begin{bmatrix} \Delta\mathbf{D} \\ \Delta\dot{\boldsymbol{\epsilon}}^{\mathrm{P}} \end{bmatrix} = \begin{bmatrix} \Delta\mathbf{F}_1 \\ \Delta\mathbf{F}_2 \end{bmatrix} \tag{23}$$

where

$$\mathbf{K}^{NM}_{\mathrm{e}} = \int_V (E^N_{ij} R_{ijkl} E^M_{kl} + \sigma_{ij}(N^M_{k,j} N^N_{k,i} - 2E^M_{ik} E^N_{jk}))\mathrm{d}V \tag{24}$$

is the elastic stiffness matrix

$$\mathbf{K}_{\mathrm{ep}}^{NM} = -\int_V m_{ij} R_{ijkl} E_{kl}^M M^N \,\mathrm{d}V \tag{25}$$

is the coupling matrix, and

$$\mathbf{K}_{\mathrm{p}}^{NM} = \int_V \left(\left(\frac{\dot{\epsilon}^{\mathrm{P}}}{\dot{E}^{\mathrm{P}2}}(m-1)q + \frac{\sigma_{\mathrm{c}}}{\dot{E}^{\mathrm{P}}} \right) M^M M^N + l_*^2 \frac{\dot{\epsilon}^{\mathrm{P}}_{,i}}{\dot{E}^{\mathrm{P}2}}(m-1) q M^M M^N_{,i} + \frac{\dot{\epsilon}^{\mathrm{P}}}{\dot{E}^{\mathrm{P}2}}(m-1)\rho_i M^M_{,i} M^N \right.$$
$$\left. + l_*^2 \frac{\dot{\epsilon}^{\mathrm{P}}_{,i}}{\dot{E}^{\mathrm{P}2}}(m-1)\rho_k M^M_{,k} M^N_{,i} + l_*^2 \frac{\sigma_{\mathrm{c}}}{\dot{E}^{\mathrm{P}}} M^M_{,i} M^N_{,i} \right) \mathrm{d}V \tag{26}$$

is the plastic stiffness matrix. The right-hand side in Eq. (23) consists of two components

$$\Delta \mathbf{F}_1^N = \int_S \Delta T_i N_i^N \,\mathrm{d}S + \Delta t \int_V E_{ij}^N R_{ijkl} m_{kl} \dot{\epsilon}^{\mathrm{P}} \,\mathrm{d}V \tag{27}$$

which is the conventional load increment vector with an added volume force, and

$$\Delta \mathbf{F}_2^N = \int_S \Delta \rho_i n_i M^N \,\mathrm{d}S - \Delta t \int_V \left(\left(m_{ij} R_{ijkl} m_{kl} \dot{\epsilon}^{\mathrm{P}} + \frac{\dot{\epsilon}^{\mathrm{P}}}{\dot{\epsilon}_0^m} \dot{E}^{\mathrm{P}m} \frac{\mathrm{d}g}{\mathrm{d}E^{\mathrm{P}}} \right) M^N + \dot{\epsilon}^{\mathrm{P}}_{,i} \dot{E}^{\mathrm{P}m} \frac{\mathrm{d}g}{\mathrm{d}E^{\mathrm{P}}} \frac{l_*^2}{\dot{\epsilon}_0^m} M^N_{,i} \right) \mathrm{d}V \tag{28}$$

which is an additional higher order load term with a subtracted volume contribution.

Since the system of equations decouples, it is possible to first solve for the displacement increments and afterwards solve for the effective plastic strain rate increments and hereby exploit the symmetry of $\mathbf{K}_{\mathrm{e}}$ and $\mathbf{K}_{\mathrm{p}}$, respectively. The integrations (24)–(28) are carried out using 3×3 point Gaussian integration.

When the displacement increments and the effective plastic strain rate increments are known, the Jaumann rate of the stress, the generalised effective stress rate and the convected rate of the higher order stress can be found from the constitutive equations (15)–(17). The increments of the Cauchy stress tensor and the higher order stress vector is then calculated by

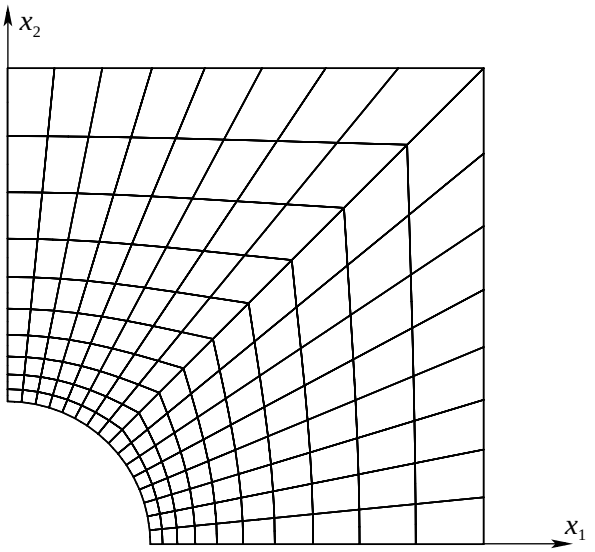

Fig. 2. Initial mesh with $a_0/b_0 = 1$ and $a_0/R_0 = 0.3$ corresponding to a volume fraction of 7.1%.

$$\Delta\sigma_{ij} = \overset{\triangledown}{\varsigma}_{ij}\Delta t + \Delta\omega_{ik}\sigma_{kj} + \sigma_{ik}\Delta\omega_{jk} - \sigma_{ij}\Delta\epsilon_{kk} \tag{29}$$

$$\Delta\tau_i = \overset{\triangledown}{\rho}_i\Delta t + \Delta e_{ik}\tau_k - \tau_i\Delta\epsilon_{kk} \tag{30}$$

Subsequently, the effective stress, σ_c, can be calculated from (12) and the effective plastic strain rate, $\dot{E}^P$, is given by (13). The conventional effective plastic strain rate, $\dot{\epsilon}^P$, and its gradient, $\dot{\epsilon}^P_{,i}$, is now obtained from Eqs. (10) and (11).

The finite element mesh used for the analyses is shown in Fig. 2.

4. Results

The material parameters used for the numerical analyses are $\sigma_0/E = 0.003$, $n = 10$, $\nu = 0.3$, $m = 0.04$ and $\dot{\epsilon}_0 = 0.005\ \mathrm{s}^{-1}$. The initial dimensions of the unit cell are specified by $a_0/b_0 = 1$ so that the voids or inclusions have equal spacings in the directions of the coordinate axes. The initial spacing of the voids or inclusions is specified by $R_0/a_0 = 0.3$ corresponding to a volume fraction of 7.1%.

Both for the material containing voids and the material containing inclusions the higher order traction is taken to vanish along the cell boundary ($\tau_i n_i = 0$). This constitutes the appropriate symmetry boundary condition for the problems analysed. Also at the free surface around the voids the higher order stress is imposed to vanish, while for the material containing inclusions the higher order boundary condition is specified by imposing vanishing plastic strain ($\epsilon^P = 0$) unless otherwise stated.

For a material with voids the overall uniaxial stress–strain curve ($\kappa = 0$) is shown in Fig. 3 for different values of the material length parameter relative to the void radius. The solid curve shows results for a conventional material ($l_* = 0$), while the dotted and dashed curves show results for gradient dependent materials with $l_*/R_0 = 0.3$ and $l_*/R_0 = 0.6$, respectively. The figure shows curves of the normalised average true stress, σ_1, in the x_1-direction as a function of the logarithmic strain, ϵ_1. The overall strain rate is equal to the reference strain rate, $\dot{\epsilon}_1 = \dot{\epsilon}_0$. It is seen from the figure how a material with small voids (or conversely a large material length parameter) shows more stiff behaviour in the plastic range. In effect, increasing the material length parameter, apparently increases the overall material yield stress and thus increases the stress level

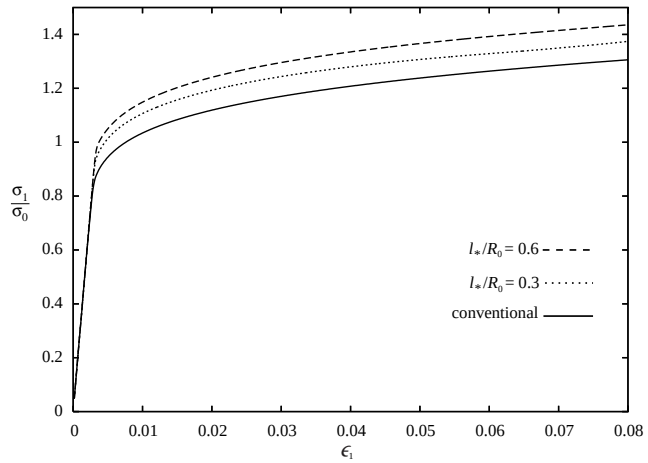

Fig. 3. Overall uniaxial stress–strain response ($\kappa = 0$) for a material with voids. The solid curve shows results from a conventional plasticity model while the dotted and dashed curves show results for plasticity models with $l_*/R_0 = 0.3$ and $l_*/R_0 = 0.6$, respectively. The overall loading rate is given by $\dot{\epsilon}_1 = \dot{\epsilon}_0$.

in the plastic range. Well inside the plastic range ($\epsilon > 0.02$) the stress level is around 6% higher for $l_*/R_0 = 0.3\%$ and 11% higher for $l_*/R_0 = 0.6$, as compared to the conventional material.

In Fig. 4 results for different overall strain rates are shown both for a conventional material and for a gradient dependent material with $l_*/R_0 = 0.6$. The overall strain rate is varied so that in addition to $\dot{\epsilon}_1 = \dot{\epsilon}_0$ also a 10 times larger and a 10 times smaller strain rate are studied. It is seen from the figure that increasing the overall strain rate for the conventional material from $\dot{\epsilon}_1 = \dot{\epsilon}_0$ to a 10 times larger value has a similar strengthening effect as accounting for gradient hardening using $l_*/R_0 = 0.6$. Moreover, the figure shows that increasing the strain rate by a factor of 10 increases the stress level in the plastic range by around 10%. This is in agreement with the increase expected on the basis of (13) for a homogeneous solid with the value of m used in the present analyses.

Fig. 5 shows the overall stress–strain curves for the material with inclusions under different levels of the overall stress ratio κ and different material length parameters. The size of the cylindrical inclusions is defined by $R_0/a_0 = 0.3$ which corresponds to a reinforcement volume fraction of approximately 7.1%. The solid curves show results for a conventional material ($l_* = 0$), while the dotted and dashed curves show results for gradient dependent materials with $l_*/R_0 = 0.3$ and $l_*/R_0 = 0.6$, respectively. The figure shows that increasing the material length scale leads to an apparent increase in the overall yield stress as was also the case for the material with voids. For all three values of the material length parameter the overall stress level for $\kappa = 0.5$ is approximately a factor of two higher than the stress level for $\kappa = 0$. This is in agreement of what would be expected for a homogeneous solid when ignoring elastic effects.

Results when varying the overall strain rate for the material with inclusions is shown in Fig. 6 for $\kappa = 0$, both for a conventional material and for a gradient dependent material with $l_*/R_0 = 0.6$. As for the material containing voids, increasing the strain rate by a factor of 10 increases the stress level by around 10%, which would be expected in the plastic range for a homogeneous material with the specific value of m used. For the material with inclusions the effect on the overall response by increasing the material length parameter from zero to $l_*/R_0 = 0.6$ is slightly larger than for the material containing voids discussed in relation to Fig. 4.

The higher order boundary condition on the interface between fibers and the matrix material is of significant importance for the overall material response of reinforced materials (see Niordson, 2003). For the

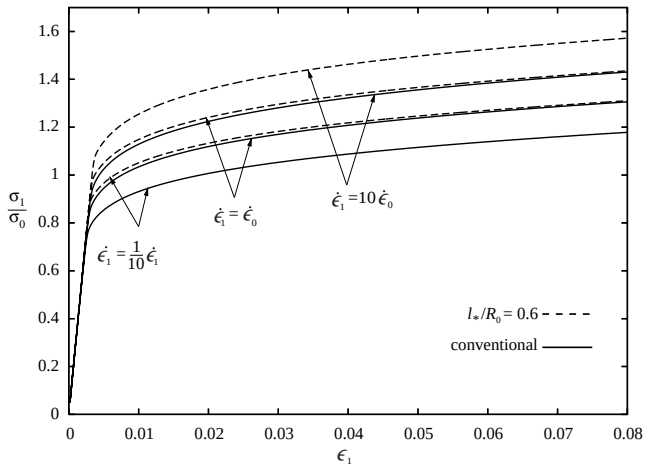

Fig. 4. Overall uniaxial stress–strain response ($\kappa = 0$) for a material with voids. For three different loading rates given by $\dot{\epsilon}_1 = \dot{\epsilon}_0/10$, $\dot{\epsilon}_1 = \dot{\epsilon}_0$ and $\dot{\epsilon}_1 = 10\dot{\epsilon}_0$, results are shown from a conventional plasticity model (solid curves) and from a gradient dependent model with $l_*/R_0 = 0.6$ (dashed curves).

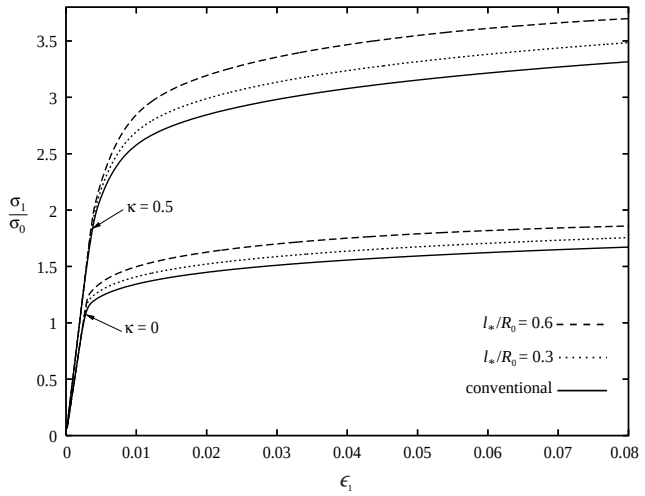

Fig. 5. Overall stress–strain response for a material with rigid inclusions and two different stress triaxialities given by $\kappa = 0$ and $\kappa = 0.5$. The solid curves show results from a conventional plasticity model while the dotted and dashed curves show results for $l_*/R_0 = 0.3$ and $l_*/R_0 = 0.6$, respectively. The overall loading rate is given by $\dot{\epsilon}_1 = \dot{\epsilon}_0$.

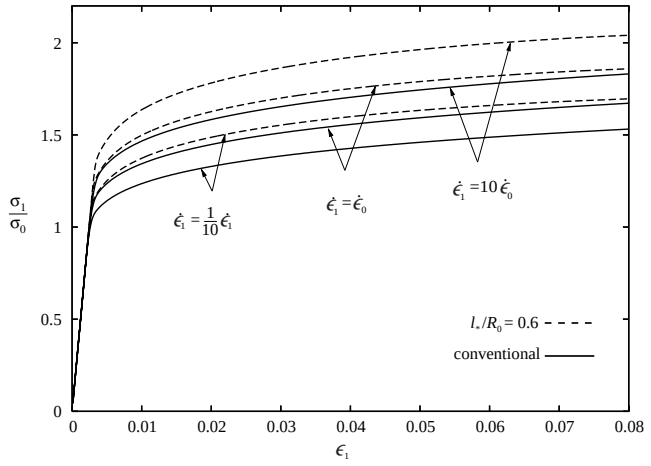

Fig. 6. Overall uniaxial stress–strain response ($\kappa = 0$) for a material with rigid inclusions. For three different loading rates given by $\dot{\epsilon}_1 = \dot{\epsilon}_0/10$, $\dot{\epsilon}_1 = \dot{\epsilon}_0$ and $\dot{\epsilon}_1 = 10\dot{\epsilon}_0$, results are shown from a conventional plasticity model (solid curves) and results from a plasticity model with $l_*/R_0 = 0.6$ (dashed curves).

results presented until now for the reinforced material a full constraint on plastic flow ($\epsilon^p = 0$) has been imposed at the interface between the matrix material and the inclusion. Fig. 7 shows results for the two extreme boundary conditions, which can be imposed at the interface. One is the full constraint on plastic flow represented by the dotted curves ($\epsilon^p = 0$), while the other is no constraint on plastic flow, as represented by the dashed curves ($\tau_i n_i = 0$). It is seen that a full constraint on plastic flow leads to an overall stiffer response when compared to no constraint on plastic flow. Furthermore, it is seen that the apparent increase in the overall material yield stress due to gradient effects, which has been observed in the results presented so far, is not so obvious when imposing vanishing higher order traction at the interface. For this

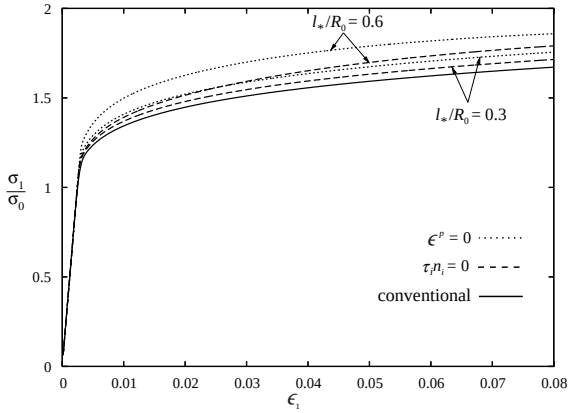

Fig. 7. Overall uniaxial stress–strain response ($\kappa = 0$) for a material with rigid inclusions using different higher order boundary conditions on the inclusion surface. The solid line shows results for a conventional model. The dashed and the dotted lines show results for the higher order traction and the plastic strain set to zero on the inclusion surface, respectively. Results are shown for two different values of l_*/R_0. The overall loading rate is given by $\dot{\epsilon}_1 = \dot{\epsilon}_0$.

boundary condition the strengthening effect seems to stem more from an increased material hardening, which takes place over a longer time in the plastic range and not predominantly in the beginning of plastic deformation.

5. Discussion

An elastic–viscoplastic material model is needed for a number of applications, where strain rate sensitivity of material behaviour is important, e.g. at rapid loading in the room temperature range, or at elevated temperatures, where time dependence of plastic flow tends to get more pronounced. This is the motivation for the constitutive model presented in the present paper.

The strain gradient plasticity theory proposed by Fleck and Hutchinson (2001) has three different material length parameters, each of which has a physical interpretation. Within this framework a theory with a single material length parameter has been formulated, closely related to the strain gradient theory of Aifantis (1984). In the finite strain generalisation developed by Niordson and Redanz (2004), all three material length parameters are incorporated, but results are also shown for the single parameter version of the theory. The present elastic–viscoplastic version of the theory has been formulated so far as a single parameter theory. Since no internal elastic–plastic boundaries exists in the elastic–viscoplastic model, no internal higher order boundary conditions need to be specified.

The results here show that both for the material containing voids and the material containing inclusions the overall stress–strain response is more stiff the larger the value of the ratio l_*/R_0 between the material length and the void or inclusion radius. This result is as expected based on the time independent strain gradient plasticity model. Also, in both cases the strain rate has been varied, and the results have shown the characteristic feature of a strain rate sensitive material that the stress levels are higher the higher the strain rate.

Due to the strongly nonlinear dependence on the stresses in (13), the solution will tend to be numerically unstable at low viscosities. To increase the stable step length at lower viscosities than those considered here, forward gradient methods (Peirce et al., 1984) would be useful.

For rigid inclusions computations using either of the two extreme sets of boundary conditions on the inclusion–matrix interface have been compared (Fig. 7). For both sets of higher order boundary conditions

the response is more stiff than that corresponding to the conventional material with no characteristic material length, as would be expected due to the gradient effects accounted for in either case. Furthermore, the boundary condition representing full constraint on plastic flow at the interface to the material that does not yield gives an overall stiffer response than the other set of boundary conditions, representing no constraint on plastic flow at the interface.

Acknowledgement

This work is financially supported by the Danish Technical Research Council in a project entitled Modeling Plasticity at the Micron Scale.

References

Aifantis, E.C., 1984. On the microstructural origin of certain inelastic models. Transactions of the ASME, Journal of Engineering Materials and Technology 106, 326–330.

Benallal, A., Tvergaard, V., 1995. Nonlocal continuum effects on bifurcation in the plane strain tension–compression test. Journal of the Mechanics and Physics of Solids 43, 741–770.

Fleck, N.A., Hutchinson, J.W., 1997. Strain gradient plasticity. In: Hutchinson, J.W., Wu, T.Y. (Eds.), Advances in applied mechanics, 33. Academic Press, New York, pp. 295–361.

Fleck, N.A., Hutchinson, J.W., 2001. A reformulation of strain gradient plasticity. Journal of the Mechanics and Physics of Solids 49, 2245–2271.

Fleck, N.A., Muller, G.M., Ashby, M.F., Hutchinson, J.W., 1994. Strain gradient plasticity: theory and experiment. Acta Metallurgica et Materialia 42, 475–487.

Fredriksson, P., Gudmundson, P., 2005. Size-dependent yield strength of thin films. International Journal of Plasticity 21, 1834–1854.

Gudmundson, P., 2004. A unified treatment of strain gradient plasticity. Journal of the Mechanics and Physics of Solids 52, 1379–1406.

Gurtin, M.E., 2003. On a framework for small-deformation viscoplasticity: free energy, microforces, strain gradients. International Journal of Plasticity 19, 47–90.

Haque, M.A., Saif, M.T.A., 2003. Strain gradient effect in nanoscale thin films. Acta Materialia 51, 3053–3061.

Huang, Y., Gao, H., Nix, W.D., Hutchinson, J.W., 2000. Mechanism-based strain gradient plasticity—II. Analysis. Journal of the Mechanics and Physics of Solids 48, 99–128.

Ma, Q., Clarke, D.R., 1995. Size dependent hardness of silver single crystals. Journal of Materials Research 10, 853–863.

Niordson, C.F., 2003. Strain gradient plasticity effects in whisker-reinforced metals. Journal of the Mechanics and Physics of Solids 51, 1863–1883.

Niordson, C.F., Redanz, P., 2004. Size-effects in plane strain sheet-necking. Journal of the Mechanics and Physics of Solids 52, 2431–2454.

Niordson, C.F., Tvergaard, V., 2005. Instabilities in power law gradient hardening materials. International Journal of Solids and Structures 42, 2559–2573.

Niordson, C.F., Tvergaard, V., in press. Size-effects on cavitation instabilities. Journal of Applied Mechanics.

Peirce, D., Shih, C.F., Needleman, A., 1984. A tangent modulus method for rate dependent solids. Computers and Structures 18, 875–887.

Stölken, J.S., Evans, A.G., 1998. Microbend test method for measuring the plasticity length scale. Acta Materialia 46, 5109–5115.

Tvergaard, V., 1976. Effect of thickness inhomogeneities in internally pressurized elastic–plastic spherical shells. Journal of the Mechanics and Physics of Solids 24, 291–304.

Tvergaard, V., Niordson, C., 2004. Nonlocal plasticity effects on interaction of different size voids. International Journal of Plasticity 20, 107–120.